CRUISE REPORT: AR07W 2023

Updated: June 2026

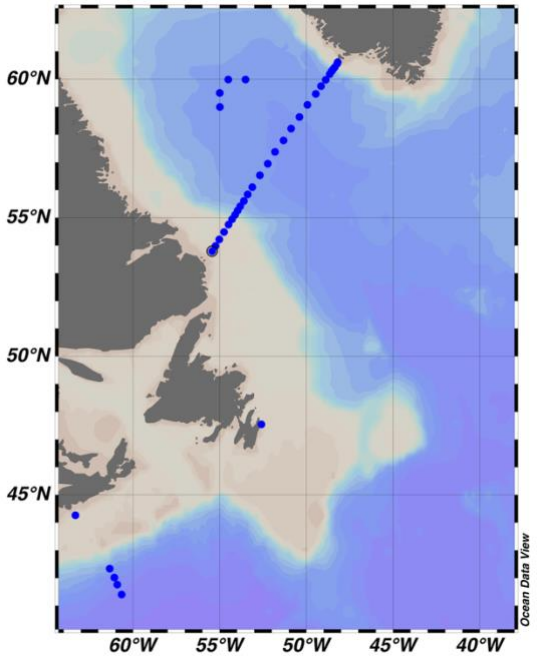

Highlights

Cruise Summary Information

Section Designation	AR07W
Expedition Designation (ExpoCode)	18QL20230524
Chief Scientists	**Marc Ringuette, BIO**
Dates	24 May – 12 June 2023
Ship	*Captain Jacques Cartier*
Ports of Call	
Geographic Boundaries	60.62°N 63.32°W 48.2°W 41.41°N
Stations	38 [Bottle]
Floats and Drifters Deployed	6 Argo floats
Moorings Deployed and Recovered	0

Contact Information:

Marc Ringuette
Bedford Institution of Oceanography

This cruise report was obtained from: Ringuette, M., Clay, S., Devred, E., Azetsu-Scott, K., Gabriel, C.-E., and Childs, D. 2025. Chemical and Biological Oceanographic Conditions in the Labrador Sea from 2019 to 2023. Can. Tech. Rep. Fish. Aquat. Sci. 3696: vi + 29 p. https://doi.org/10.60825/hy8b-9e23

Report assembled by Savannah Lewis

Chemical and Biological Oceanographic Conditions in the Labrador Sea from 2019 to 2023

Marc Ringuette, Stephanie Clay, Emmanuel Devred, Kumiko Azetsu-Scott, Carrie-Ellen Gabriel, and Darlene Childs

Fisheries and Oceans Canada
Science Branch, Maritimes Region
Bedford Institute of Oceanography
P.O. Box 1006
1 Challenger Drive
Dartmouth, NS B2Y 4A2

2025

Canadian Technical Report of
Fisheries and Aquatic Sciences 3696

Fisheries and Oceans Canada | Pêches et Océans Canada

Canada

Canadian Technical Report of Fisheries and Aquatic Sciences

Technical reports contain scientific and technical information that contributes to existing knowledge but which is not normally appropriate for primary literature. Technical reports are directed primarily toward a worldwide audience and have an international distribution. No restriction is placed on subject matter and the series reflects the broad interests and policies of Fisheries and Oceans Canada, namely, fisheries and aquatic sciences.

Technical reports may be cited as full publications. The correct citation appears above the abstract of each report. Each report is abstracted in the data base *Aquatic Sciences and Fisheries Abstracts*.

Technical reports are produced regionally but are numbered nationally. Requests for individual reports will be filled by the issuing establishment listed on the front cover and title page.

Numbers 1-456 in this series were issued as Technical Reports of the Fisheries Research Board of Canada. Numbers 457-714 were issued as Department of the Environment, Fisheries and Marine Service, Research and Development Directorate Technical Reports. Numbers 715-924 were issued as Department of Fisheries and Environment, Fisheries and Marine Service Technical Reports. The current series name was changed with report number 925.

Rapport technique canadien des sciences halieutiques et aquatiques

Les rapports techniques contiennent des renseignements scientifiques et techniques qui constituent une contribution aux connaissances actuelles, mais qui ne sont pas normalement appropriés pour la publication dans un journal scientifique. Les rapports techniques sont destinés essentiellement à un public international et ils sont distribués à cet échelon. II n'y a aucune restriction quant au sujet; de fait, la série reflète la vaste gamme des intérêts et des politiques de Pêches et Océans Canada, c'est-à-dire les sciences halieutiques et aquatiques.

Les rapports techniques peuvent être cités comme des publications à part entière. Le titre exact figure au-dessus du résumé de chaque rapport. Les rapports techniques sont résumés dans la base de données *Résumés des sciences aquatiques et halieutiques.*

Les rapports techniques sont produits à l'échelon régional, mais numérotés à l'échelon national. Les demandes de rapports seront satisfaites par l'établissement auteur dont le nom figure sur la couverture et la page du titre.

Les numéros 1 à 456 de cette série ont été publiés à titre de Rapports techniques de l'Office des recherches sur les pêcheries du Canada. Les numéros 457 à 714 sont parus à titre de Rapports techniques de la Direction générale de la recherche et du développement, Service des pêches et de la mer, ministère de l'Environnement. Les numéros 715 à 924 ont été publiés à titre de Rapports techniques du Service des pêches et de la mer, ministère des Pêches et de l'Environnement. Le nom actuel de la série a été établi lors de la parution du numéro 925.

Canadian Technical Report of
Fisheries and Aquatic Sciences 3696

2025

CHEMICAL AND BIOLOGICAL OCEANOGRAPHIC CONDITIONS IN THE LABRADOR SEA FROM 2019 TO 2023

by

Marc Ringuette, Stephanie Clay, Emmanuel Devred, Kumiko Azetsu-Scott, Carrie-Ellen Gabriel,
and Darlene Childs

Fisheries and Oceans Canada
Science Branch, Maritimes Region
Bedford Institute of Oceanography
P.O. Box 1006
1 Challenger Drive
Dartmouth, NS B2Y 4A2

Cat. No. Fs97-6/3696E-PDF ISBN 978-0-660-77139-7 ISSN 1488-5379
https://doi.org/10.60825/hy8b-9e23

Correct citation for this publication:

Ringuette, M., Clay, S., Devred, E., Azetsu-Scott, K., Gabriel, C.-E., and Childs, D. 2025. Chemical and Biological Oceanographic Conditions in the Labrador Sea from 2019 to 2023. Can. Tech. Rep. Fish. Aquat. Sci. 3696: vi + 29 p. https://doi.org/10.60825/hy8b-9e23

CONTENTS

ABSTRACT

Ringuette, M., Clay, S., Devred, E., Azetsu-Scott, K., Gabriel, C.-E., and Childs, D. 2025. Chemical and Biological Oceanographic Conditions in the Labrador Sea from 2019 to 2023. Can. Tech. Rep. Fish. Aquat. Sci. 3696: vi + 29 p. https://doi.org/10.60825/hy8b-9e23

The Atlantic Zone Off-Shelf Monitoring Program samples the AR7W line annually. This report summarises trends from 2019-2023 for three regions: AR7W-W (Labrador shelf and slope), AR7W-C (central Labrador Sea), and AR7W-E (Greenland shelf and slope). Samples revealed a continued increase in dissolved inorganic carbon and a decrease in pH from 2019 to 2023. Mean concentration of CFC-12 decreased in 2020, and SF_6 continued its steady increase. Mean temperature from 0-100 m in the Labrador Sea was above normal in 2019, below normal on the next mission (2022), and near or above normal in 2023. Surface (0-100 m) nutrients were mainly below normal from 2019-2023, which could be attributed to mission timing. However, below-average deep nutrients (>100 m, less impacted by sampling timing) suggests a profound change in the biogeochemistry of the Labrador Sea. Integrated (0-100 m) chlorophyll-a was below normal in 2019 and in AR7W-E in 2022-2023, but above normal elsewhere, with a record high value in AR7W-C in 2022 caused by an unusually large bloom of *Phaeocystis spp.*. Satellite data revealed high variability in the timing of the spring and fall blooms and surface average chlorophyll-a concentration. Mesozooplankton abundances showed high interannual variability since 2019.

RÉSUMÉ

Ringuette, M., Clay, S., Devred, E., Azetsu-Scott, K., Gabriel, C.-E., and Childs, D. 2025. Chemical and Biological Oceanographic Conditions in the Labrador Sea from 2019 to 2023. Can. Tech. Rep. Fish. Aquat. Sci. 3696: vi + 29 p. https://doi.org/10.60825/hy8b-9e23

Le programme de monitorage hauturier de la zone atlantique échantillonne chaque année la ligne AR7W. Le présent rapport résume les tendances observées entre 2019 et 2023 dans trois régions: AR7W-W (plateau et talus du Labrador), AR7W-C (centre de la mer du Labrador) et AR7W-E (plateau et talus du Groenland). Les échantillons ont révélé une augmentation continue du carbone inorganique dissous et une diminution du pH de 2019 à 2023. La concentration moyenne de CFC-12 a diminué en 2020, et la concentration de SF_6 a continué à augmenter régulièrement. La température moyenne de 0 à 100 m dans la mer du Labrador était supérieure à la normale en 2019, inférieure à la normale lors de la mission suivante (2022), et supérieure ou proche de la normale en 2023. Les nutriments de surface (0-100 m) étaient principalement inférieurs à la normale de 2019 à 2023, ce qui pourrait être attribué au calendrier des missions. Cependant, les nutriments profonds inférieurs à la moyenne (>100 m, moins influencés par la date d'échantillonnage) suggèrent un changement profond dans la biogéochimie de la mer du Labrador. La chlorophylle-a intégrée (0-100 m) était inférieure à la normale en 2019 et dans AR7W-E de 2022 à 2023, mais supérieure à la normale ailleurs, avec une valeur record dans AR7W-C en 2022 qui a été causée par une efflorescence inhabituellement importante de *Phaeocystis spp.*. Les données satellitaires ont révélé une grande variabilité dans l'initiation des efflorescences de printemps et d'automne et dans la concentration moyenne de chlorophylle-a à la surface. Les abondances de mésozooplancton ont montré une forte variabilité interannuelle depuis 2019.

1 Introduction

The Labrador Sea is a deep basin nested between Labrador and Greenland with a cyclonic circulation pattern that leads to the mixing of Arctic and North Atlantic waters. The Baffin Island and Labrador currents transport cold and less-saline Arctic water southward along the Canadian coast (Wang et al. 2016). On the eastern side, the West Greenland Current brings warmer, more-saline waters northward, along the Greenland coast into the Baffin Bay, where it meets the Labrador Current. (See Lozier et al. (2019) and Yashayaev and Loder (2017) for a detailed description of the Labrador Sea circulation.) By the end of winter, the cooling of the upper layer results in an increase of surface density, enabling wind-driven mixing and convection to reach great depths (1500 to 2000 m), thus ventilating the deeper ocean with atmospheric gases while pumping nutrients from the deep waters to the surface. The intensity of this phenomenon varies with environmental factors, including atmospheric forcing, freshwater runoff from adjacent glaciers, precipitation, intrusion of warm and saline inflow from the adjacent North Atlantic, and intrusion of cold and fresh water from the Arctic Ocean. In turn, this deep mixing strongly impacts heat flux, stratification, and by extension, the chemical balance and biological productivity of the Labrador Sea. Consequently, changes in the physical and chemical environment of the aphotic zone influence both plankton community composition and annual biological production cycles, including fish and higher trophic levels.

About one quarter of the carbon dioxide ($\mathrm{CO_2}$) released by human activities is taken up by the global ocean (Sabine et al. 2004), altering ocean chemistry, and correspondingly, the marine carbonate system. The Labrador Sea hosts a strong “solubility pump”, whereby anthropogenic $\mathrm{CO_2}$ sequestrated from the atmosphere is transported to the deep ocean through chemical and physical processes. Globally, the dissolution of anthropogenic $\mathrm{CO_2}$ has decreased ocean pH by 0.1 units over the past 200 years, resulting in a 30% increase in acidity (Caldeira and Wickett 2003). If global emissions of $\mathrm{CO_2}$ remain at their present rate, ocean pH is predicted to drop by an additional 0.3 units by 2100. The oceans have not experienced such a rapid pH decrease (ocean acidification), or one of such a high magnitude, for at least 20 million years (Feely et al. 2004), raising serious concerns about the ability of marine ecosystems to adapt. The major impact of decreasing pH will be felt by organisms that form calcium carbonate ($\mathrm{CaCO_3}$) shells and skeletons, because rising acidity increases the solubility of $\mathrm{CaCO_3}$. Since $\mathrm{CaCO_3}$ shells and skeletons are naturally more soluble at lower temperatures and higher pressures, high latitudes and deep water ecosystems, such as the one encountered in the Labrador Sea, are more vulnerable to the added stress of ocean acidification than those at intermediate latitudes. Ocean acidification also influences the capacity of the ocean to take up $\mathrm{CO_2}$ from the atmosphere. Furthermore, rapid environmental changes, such as receding sea-ice extent and enhanced hydrological cycles, may amplify these problems.

Transient tracers dichlorodifluoromethane (CFC-12) and sulfur hexafluoride ($\mathrm{SF_6}$) are used to study ocean circulation, ventilation, and mixing processes. Specifically, they are used to study ventilation rates and age determination of water masses. As the Labrador Sea is the site of direct uptake of these tracers by deep convection during winter, these measurements provide the boundary conditions for the global network of tracer observations, which are used to trace ocean circulation pathways such as spreading of North Atlantic Deep Water. These tracers are also used to estimate anthropogenic $\mathrm{CO_2}$ storage and track their changes (Haine and Hall 2002; Hall et al. 2002; Raimondi et al. 2021).

Since 1990, as part of the World Ocean Circulation Experiment (WOCE), the Ocean and Ecosystem Sciences Division (OESD) at the Bedford Institute of Oceanography (BIO) has carried out an annual occupation, usually in the spring, of the AR7W (Atlantic Repeat Hydrography Line 7 West) oceanographic section across the Labrador Sea (Figure 1). Soon after its inception, the program morphed into Fisheries and Oceans Canada (DFO) Atlantic Zone Off-shelf Monitoring Program (AZOMP), following the OESD's overarching objectives to: 1) characterize and understand the causes of ocean variability at seasonal, inter-annual, and inter-decadal scales; 2) provide adequate data to monitor the health of the marine ecosystem and support decision-making based on scientific evidence; and 3) to build historical databases to address future issues. The program also contributes to the international Global Climate Observing System (GCOS) and the Climate Variability (CLIVAR) component of the World Climate Research Program (WCRP), the Global Ship-based Hydrographic Investigations Program (GO-SHIP), the Global Ocean Acidification Observing Network (GOA-ON), the United Nations Sustainable Development Goals 14.3.1 (UN SDG14.3.1), the Global Ocean Data Analysis Project (GLODAP), and it reports annually with an environmental synopsis to the Northwest Atlantic Fisheries Organization (NAFO).

The AR7W section spans approximately 900 km across the southern edge of the Labrador Sea, from the Labrador shelf (near 53°N) to the Greenland shelf (near 61°N) (Figure 1). The annual AZOMP multidisciplinary survey of the Labrador Sea primarily consists of AR7W occupations and deployments/recoveries of moorings and Argo floats. The ideal timing of the mission in May aims to capture the fading winter-deep-convection signal and the beginning of the phytoplankton bloom and productivity season, while avoiding possible sea-ice on the Labrador shelf early in the spring. Sampling the peak of the spring bloom is uncertain given its large inter-annual variability in timing, duration and spatial extent, but early cruise dates in recent decades have captured its initiation with the exception of the 2020 mission, which occurred in July-August under nutrient-limited conditions (Table 1, Figure 2). With nearly three decades of measurements, the time series allows examination of decadal trends in all key ecosystem variables (i.e, temperature, nutrients, plankton biomass and abundance).

The AR7W transect crosses two productive shelves (Labrador and Greenland shelves) and the central Labrador Sea, where phytoplankton production is subject to local forcing (eddies, mixing-stratification) that drive phytoplankton biomass and community structure. In the central Labrador Sea, light limits primary production for most of the year (Harrison and Li 2008; Fragoso et al. 2016), while a shallow mixed layer, and relatively low nitrate concentration, limit phytoplankton growth on the Labrador shelf following the spring bloom. Phytoplankton growth, in particular diatoms, also seemed to be limited by availability of silicate in the central Labrador Sea (Harrison and Li 2008). These conditions support the emergence of small flagellates such as *Phaeocystis pouchetii* in the northern and eastern region of the Labrador Sea, which can form large blooms under favorable conditions (Fragoso et al. 2016). In recent years, large blooms of *Phaeocystis spp.* have also been observed in the western part of the central Labrador Sea (Devred et al. 2024). The Labrador shelf, influenced by Arctic waters, is dominated by polar diatom species (*Thalassiosira spp.*, *Chaetoceros spp.*, and *Bacteriosira bathyomphala*) and species associated with sea-ice (*Porosira glacialis* and *Fossula arctica*). Primary production patterns and mesoscale features leave their imprint on the mesozooplankton distribution and abundance (Yebra et al. 2009). One species of copepod, *Calanus finmarchicus*, dominates the mesozooplankton biomass throughout the central region of the Labrador Sea, while on the shelves, two Arctic *Calanus* species, *C. glacialis* and *C. hyperboreus*, are equally important (Head et al. 2003). *C.*

finmarchicus abundance shows regional variations that are generally consistent from year-to-year and are related to differences in the timing of life-cycle events, which are influenced by environmental conditions, including spring bloom dynamics.

This report describes the biogeochemical state of the Labrador Sea between spring 2019 and spring 2023. Data presented in this report come from: 1) annual surveys carried out over 2-week periods, typically between early May and early June, but due to the unavailability and subsequent decommissioning of CCGS Hudson, the timing of the surveys in 2020 occurred in summer between late July and early August and there was no mission in 2021 (Table 1); and 2) satellite remote-sensing of daily observations of ocean colour converted into chlorophyll-a (chl-a) concentration.

2 Data and Methods

2.1 In situ samples collection

2.1.1 Core stations

The core stations (Figure 1) remain the priority of the monitoring program to ensure geographical consistency over time when reporting on the data. The main goal of the sampling is to obtain a complete suite of measurements at selected locations from surface to bottom to characterize the physical and chemical properties of the entire water column and the biological properties in the upper layers (0 to 100 m). The CTD (Conductivity, Temperature, Depth)-rosette system used to carry out measurements and water collection includes twenty-four 24 L Niskin bottles and a core of twinned sensors to measure temperature, salinity and oxygen, as well as additional sensors to measure fluorescence (both chl-a and Colored Dissolved Organic Matter (CDOM)), pH, light attenuation, Photosynthetically Active Radiation (PAR) and current velocity (LADCP). Water samples are collected at 24 depths distributed over the entire water column to measure transient gases (CFC-12 and $\mathrm{SF_6}$), oxygen, partial pressure of carbon dioxide ($\mathrm{pCO_2}$), Total Inorganic Carbon (TIC), alkalinity, pH, nutrients, and salinity. In addition to the previous measurements, four surface-layer depths (2, 25, 50 and 100 m) are sampled for chl-a and cell abundance (Flow Cytometry). The 2 m depth is sampled for phytoplankton absorption and pigment composition, particulate carbon, and CDOM absorption. Once the CTD-Rosette is onboard, the collection of water from the Niskin bottles is carried out as listed previously (i.e., gases first and phytoplankton last) from bottom to surface waters to minimize the loss of transient tracers and other gases during sampling. All variables were sampled and analyzed following GO-SHIP protocols (Mitchell et al. 2002; Hood et al. 2010). In addition to water sampling from the Niskin bottles, mesozooplankton are collected in vertical net hauls in the upper 100 m using a 0.75 m diameter ring net fitted with a 200 µm mesh, and 0.5 m diameter ring net with a 76 µm mesh size. A detailed description of the processing of the physical oceanographic data is presented in Yashayaev et al. (2021).

When time allows, extra stations are added between core stations in order to increase the spatial resolution of the sampling. However, on these stations only measurements from the sensors located on the CTD-Rosette are recorded and water is not collected unless requested

by programs outside the core program. At these stations, the CTD-Rosette system is lowered to the ocean bottom to profile the entire water column. Note that in the current report, only data collected on the core and biological stations are included.

2.1.2 Biological stations

The purpose of these stations is to increase the vertical resolution compared to core stations and to carry out Photosynthesis-Irradiance (P-I) 14C-uptake experiments with phytoplankton (water) samples. In these experiments, 33 aliquots of phytoplankton from two depths (surface and close to the deep chl-a maximum) are incubated with 14C-bicarbonate at in situ temperatures and 30 light levels (+ 3 dark bottles) for approximately 3 hours. The P-I measurements are used to estimate primary production according to Platt and Jassby (1976). The actual location of the biological stations is not critical, so the vessel is stopped mid-morning during transit between stations, in order to start the incubations around noon, local time, to ensure consistency of the method. Because the biological stations focus on the upper layers of the water column, the CTD sensor is only lowered to 200 m, allowing for a greater vertical resolution of all the biogeochemical parameters. Bottles are closed at 2, 10, 20, 30, 40, 50, 60, 80, 100, and 150 m, with an extra bottle at the depth of the deep chl-a maximum, as revealed by the in situ fluorescence sensor. In general, a total of seven biological stations are sampled, which are spread along the AR7W transect: two on the Labrador shelf, three in the central Labrador Sea, and two on the Greenland shelf.

2.2 Discrete variable measurements and data collection

In the current report, we present the data for a subset of the measurements listed in section 2.1: Transient tracers, TIC, pH, CTD temperature (0-100 m), nutrients, chl-a, and mesozooplankton abundances. The remaining datasets are available in the Canadian Integrated Ocean Observing System (CIOOS, https://cioos.ca) and Open Data (https://search.open.canada.ca). Links can be provided upon request to the corresponding author.

2.2.1 Transient tracers SF_6 and CFC-12

Prior to analysis, seawater samples from the rosette were drawn directly into 250 mL glass syringes and were stored at approximately 4 ℃ in a low-temperature incubator for up to 12 hours. Immediately before analysis, the samples were warmed to approximately 20 ℃ in a water bath then injected into the purge vessel of a custom-made purge-and-trap system, where dissolved gases were stripped from the sample in a stream of ultra-high-purity nitrogen with a flow rate of 140 mL per minute. The SF_6 and CFC-12 gases were quantitatively retained in a trap comprised of 30 cm of 1/16" stainless steel tubing packed with 100–120 mesh Carboxen 1000, held at -70 ℃ over liquid nitrogen. After each 7 minute purge cycle, the trap was heated to 180 ℃ with a low-voltage electric current and the desorbed gases directed to a Varian gas chromatograph equipped with an electron-capture detector. SF_6 and CFC-12 were separated on a one-meter pre-column packed with Porasil B and a three-meter main column packed with

Molecular Sieve 5A held isothermally at 100 ℃. Total run-time was 11.5 minutes for each sample. The chromatographic sample peaks were quantified with Varian Galaxie software and the analytical system calibrated at least once each day using an air standard supplied by the Climate Monitoring and Diagnostics Laboratory of the National Oceanic and Atmospheric Administration (CMDL/NOAA), Boulder, Colorado. Analytical precision, as determined by repeated standard injections, was around ± 2% for SF_6 and ± 0.7% for CFC-12. (Punshon et al. 2016)

2.2.2 Total Inorganic Carbon (TIC), Total Alkalinity (TA), and pH

Samples for Total Inorganic Carbon (TIC) and Total Alkalinity (TA) were collected in 500 mL borosilicate glass bottles. Before 2013, TIC and TA were measured onboard within six hours of sample collection. After 2013, samples were preserved with mercuric chloride following best practices described by Dickson et al. (2007) and stored at room temperature until analysis at BIO's chemical laboratory. TIC was measured using gas extraction and coulometric titration with photometric endpoint detection (Johnson et al. 1987). TA was measured by open-cell potentiometric titration with full-curve Gran Point determination using a Titrando dosimat with Tiamo software, along with a sample delivery system that was built in-house. Certified Reference Material (CRM) (supplied by Professor Andrew Dickson, Scripps Institution of Oceanography, San Diego, USA) was analyzed in duplicate every 20 samples to ensure accuracy.

Spectrophotometric pH measurements, using an Agilent 8453 UV-Vis spectrophotometer, began in 2009. Samples were collected in 60 mL borosilicate glass tubes, stored at 4 ℃, and analyzed onboard within six hours of collection following best practices (Dickson et al. 2007). Detailed methods for TIC, TA, and pH analyses are described in Punshon et al. (2019) and Raimondi et al. (2019).

pH values were calculated from TIC and TA measurements using CO2SYS, applying the dissociation constants of Lueker et al. (2000), and are presented here to ensure consistency throughout the study period. However, in 2012 and 2014, pH values were derived using direct pH measurements and TIC due to a TA instrument failure. All pH values are reported on the total scale.

2.2.3 Surface temperature (Surface to 100 m)

CTD profiles were collected on both the downcast and upcast from surface to near bottom (often several thousand meters deep). While the downcast provides the temperature profile across all depths, in this report we only used the temperature data at the discrete depths at which water was collected for biological sampling during the CTD upcast (see section 2.1). The rosette is stopped in the water column at the depths where bottle data is collected and allowed to acclimate for a minimum of one minute. CTD sensor data is recorded from the scan that occurs at the exact moment when the bottle is closed, and the rosette then resumes its ascent. The temperature data is retrieved from the CTD record at the time of bottle firing and reported in ℃.

2.2.4 Nutrients

Nutrient measurements were made using a SEAL Analytical continuous-flow AutoAnalyzer 3 (AA3) and concentrations are expressed in micromoles per liter. The analytical methods have been modified from the historically used Technicon II: Technicon for Seawater Analysis (Silicate 186 72W, Phosphate 155 71W, Nitrate/Nitrite 158 71W) (Kérouel and Aminot 1997) so as to remain compatible with methods described in the nutrient section of The GO-SHIP Repeat Hydrography Manual (Becker et al. 2020). Duplicate nutrient samples were drawn into 10 ml collection vials directly from the rosette without using tubing, with technicians wearing vinyl gloves to avoid contamination. Samples were stored at 4 ℃ and analyzed within 12 hours. Five dissolved inorganic nutrients were analyzed, namely, nitrate plus nitrite ($\mathrm{NO_3}$ + $\mathrm{NO_2}$), nitrite ($\mathrm{NO_2}$), phosphate ($\mathrm{PO_4}$), silicate ($\mathrm{SiO_4}$), and ammonium ($\mathrm{NH_4}$). Note that in 2023, nutrients were frozen and analyzed upon return to BIO due to a lack of laboratory space in the CCS Jacques Cartier preventing the installation of the auto-analyser.

The instrument was calibrated for every analytical run, using a six-point calibration curve from pre-made solutions diluted using artificial seawater of same salinity as the samples, distributed over the concentration range for each nutrient. The analysis was followed by a drift standards analysis and blank samples to determine the method's detection limits. The baseline was re-assessed every 12 sample duplicates (i.e., every 6 samples). The pH of the imidazole buffer was monitored to ensure optimal pH levels (i.e. approximately 7.83-7.85) for the nitrate plus nitrite analyses, and adjusted as needed using hydrochloric acid, thus improving the lifespan and stability of the cadmium reduction column. Ultimately, this method diminished drift issues observed in the past between analytical runs.

The quality of these analyses was validated by analyzing a CRM for nutrients produced by KANSO Co., Ltd, Japan. There is no existing reference material for ammonium in seawater, although CRM values were tracked for consistency.

2.2.5 In situ chlorophyll-a concentration

Phytoplankton biomass is represented by the concentration of its main pigment, chl-a, which was measured using Turner fluorometry (Yentsch and Menzel 1963). Details of the protocol and method can be found in Mitchell et al. (2002). In brief, two replicates of 100 mL aliquots of seawater were drawn from each sampling depth and filtered via vacuum filtration (PSI < 10) onto 25 mm glass fiber filters (GF/F). The GF/Fs were immediately deposited into separate scintillation vials containing 10 mL of 90% acetone, which were kept at -20 ℃ for at least 24 hours to ensure extraction of all the chl-a pigments. Following the extraction period, the aliquots were warmed to room temperature and transferred into fluorometer cuvettes (glass test tubes). The extracts were exposed to blue light (excitation wavelengths) in the fluorometer, which leads them to emit red light. This red light is detected and quantified by a photomultiplier (Holm-Hansen et al. 1965). Chloropigments other than chl-a (e.g., chlorophyll-b, chlorophyll-c1, -c2, and -c3) can contribute to the overall fluorescence signal, but their contribution is generally minor. Chl-a degradation products (a-type phaeopigments associated with senescent phytoplankton or zooplankton fecal pellets) may sometimes be present in a sample and contribute to the fluorescent signal. To account for their contribution, after taking the first

fluorescence measurement, samples were acidified, which converts chl-a into phaeophytin-a. A conversion factor was then applied to retrieve the concentrations of both the chl-a and a-type phaeopigments (Welschmeyer 1994).

2.2.6 Satellite-derived chlorophyll-a concentration

In addition to in situ measurements, chl-a concentrations were derived using satellite ocean colour. This mode of observation provides information on phytoplankton biomass at synoptic scales and daily frequency (assuming clear skies). These satellite-derived data are used to complement the in-situ observations by providing context to the seagoing missions, including a suite of metrics to characterize the phytoplankton spring bloom (see section 2.3.5). Satellite data presented in this document are retrieved using the MODerate Resolution Imaging Spectroradiometer (MODIS) on the Aqua platform launched by the National Aeronautic Space Administration (NASA) in 2002. While NASA has launched several satellites since 1998, in this report only data from the MODIS sensor are presented in order to have a consistent and climate-compatible time series of chl-a concentrations that is free of satellite inter-calibration issues. MODIS is the satellite with the longest continuous time series—the first full year of data was 2003 and it is still operating.

For this report, global daily level-3 binned data at 4 km resolution were downloaded from NASA Ocean Biology Processing Group and data were extracted for the three regions of interest, namely, AR7W-West (AR7W-W, -55.7°E to -53.7°E and 53.6°N to 55.5°N), AR7W-Central (AR7W-C, -53.7°E to -48.8°E and 55.5°N to 60.1°N), and AR7W-East (AR7W-E, -48.8°E to -48.1°E and 60.1°N to 60.7°N) (Figure 1). The boundaries of these boxes were designed to delineate the main regions along the AR7W line: Labrador shelf and slope, central Labrador Sea, and the Greenland shelf and slope. In previous reports, these polygons were referred to as the Labrador Shelf (LAS), Central Labrador Sea (CLS), and the Greenland Shelf (GS), respectively, but have been renamed to reduce confusion when referring to the shelves or the central Labrador Sea as a whole. Remote sensing reflectances were used to generate POLY4 chl-a (Clay et al. 2019), a modified version of the band ratio model OCx (O'Reilly et al. 1998) with regionally-tuned coefficients to correct a bias observed in the Northwest Atlantic. Mapped POLY4 data for the Northwest Atlantic are available online, hosted by CIOOS Atlantic (https://cioosatlantic.ca/erddap/info/bio_remote_sensing_modis_aqua_chl_poly4/index.html).

2.2.7 Mesozooplankton

Mesozooplankton were collected using vertical net hauls in the upper 100 m, where 95% of the biomass in spring-summer occurs (Astthorsson and Gislason 2003), using a 0.75 m diameter ring net fitted with a 200 µm mesh size and 0.5 m diameter ring net with a 76 µm mesh size. The cod-end was attached via a clamp to a weighted hydro-wire and the towing bridle was attached to a crossbow mounted on the wire, at a height above the cod-end such that the net was held vertically. In this configuration, zooplankton were only collected as the net was towed upwards. The towing speed was about 0.5 $\mathrm{m\ s^{-1}}$ and the volume of water sampled was assumed to be the volume of the cylinder sampled by the net, until 2010, when the filtered volumes started to be measured using a Danemark K/C flowmeter. The flowmeter was equipped with a back-spin pin,

to prevent the impeller from spinning during the descent of the net, so that it only measured flow during the ascent. Samples were preserved in 2% formalin. For *C. finmarchicus*, *C. hyperboreus*, and *C. glacialis*, specimens were identified and enumerated to the level of species and stage, and size-frequency distributions of sizes-at-stage were constructed for all stages at each station. To track anomalies in reproduction events and population growth, the Population Development Index (%PDI) was calculated as the ratio of young copepodite stages (CI-CIII) over the total abundance, expressed as a percentage (Head et al. 2008). Other taxa were identified to the level of species (sometimes to stage), genus, or group, depending on their abundance in the samples. Meaningful abundances were obtained when a minimum of 300 organisms, and a minimum of 200 *Calanus spp.*, were counted to allow assessment of community structure and *Calanus* population growth/development, respectively.

2.3 Computational methods

2.3.1 Spatio-temporal binning

All data are aggregated following a spatio-temporal scheme to summarise the information in simple metrics. The biological and physical data are summarized over the three main regions of interest defined in section 2.2.6 (AR7W-W, AR7W-C, and AR7W-E, see Figure 1). For the chemical data, statistics were limited to samples collected within 150 to 500 m depth and stations from 56°N to 59.1°N along the AR7W line. These samples were considered representative of the Newly Ventilated Labrador Sea Water (NV-LSW) as they are less impacted by seasonal variability than surrounding waters (Azetsu-Scott et al. 2003).

All nutrients and chl-a concentrations were integrated over selected depth ranges, namely, chl-a from 0 to 100 m, surface nutrients from 0 to 100 m, and deep nutrients from the first depth below 100 m to bottom. Temperatures were averaged from 0 to 100 m. Zooplankton values correspond to the integrated abundances in the water column (0–100 m) since collection was carried out using vertical net tows (see section 2.2.7). Following the vertical binning, the data were averaged by region and year.

2.3.2 Time series

AZOMP sampling period is dictated by the Canadian Coast Guard operational needs and ship availability, which has been challenging since the late 2010's due to mechanical issues with the research vessel CCGS Hudson. From 2008 to 2018 (except 2013), AZOMP missions have started slightly early each year, with about 25 days difference over the entire period (Figure 2). The timing of the mission has been highly variable since 2019 with the chartering of oceanographic vessels to conduct the mission, and the 2021 mission was skipped entirely due to lack of ship availability. In addition, the COVID pandemic in 2020 prevented the chartering of foreign vessels and the mission was only possible on the CCGS Amundsen at a later date in July – August (Table 1). As a result, measurements collected during that mission were not included in the analysis to avoid possible bias. This leaves data from 2019, 2022, and 2023 over the period of interest in the current report.

2.3.3 Chemistry trends

Tracer, TIC, and pH data were averaged annually over the NV-LSW and presented as time series in Figures 3 and 4. Linear trends were calculated for SF_6, TIC, and pH using an ordinary least squares method, as each exhibited monotonic trends over time. Note that pH is a logarithmic expression of hydrogen ion concentration, which is the actual measure of acidity. Because of this, a unit change in pH corresponds to a tenfold change in $[\mathrm{H}^+]$, meaning that shifts at lower pH levels reflect much larger changes in acidity than equivalent shifts at higher pH.

2.3.4 Scorecards

Annual anomalies for temperature, surface and deep nutrients, chl-a concentration, mesozooplankton abundance, and satellite ocean colour metrics were calculated as the deviation of an individual year from the mean of the annual estimates over a reference period (defined below), and expressed as normalized quantities (i.e., by dividing by the standard deviation of the annual estimates over the same period):

$$A_y = (M_y - M_r)/\sigma_r \tag{1}$$

where A_y is the anomaly for a given property in a given year (y) and region, M_y is the annual mean, M_r is the reference period mean and σ_r is the standard deviation for the reference period. The reference period was defined as 2003-2020 for satellite data according to data availability, and 1999-2020 for in situ data. This method was selected because it provides good estimates of anomalies and trends for data with large gradients and gaps (Jones and Hulme 1996). Note that years when sampling occurred after day of year 170 (during summer, see 1998, 1999, 2002, 2003, and 2020 in Figure 2) were excluded from calculation of the in situ data reference period and omitted from the scorecards (Figures 5-8 and 10). These samples, collected in the summer rather than spring during the typical bloom period, would reflect a different dynamic and skew the climatology. Due to the lack of mission in 2017 and 2021, these cells are also greyed out in the scorecards.

2.3.5 Spring bloom metrics

Metrics were derived from satellite chl-a using the PhytoFit R shiny app (Clay et al. (2021), https://cioosatlantic.ca/phytofit). Data were $\log_{10}$-transformed to allow better modelling of the exponential increase in chl-a at the initiation of the bloom. Daily averages and standard deviations were calculated within each of the three Labrador Sea polygons (AR7W-W, AR7W-C, and AR7W-E), filtering pixels outside ±3 standard deviations from the mean. Days with less than 20 % coverage were excluded from the time series, and the remaining points were smoothed using the LOESS method (locally-estimated scatterplot smoothing) as implemented in R (loess() function) with a span window of 0.2 (a parameter that controls the degree of smoothing) and weighted by percent coverage. A symmetric shifted Gaussian was fitted to the smoothed points with nonlinear least squares regression using the nlsLM() function of the minpack.lm package in R (Elzhov et al. 2023), and the chl-a baseline was allowed to vary linearly as a function of time. The Gaussian fits were restricted to days 85 to 299, and the day of initiation and day of

maximum concentration were restricted to day ranges 85-226 and 108-247, respectively to avoid classification of small early peaks of the spring bloom.

In previous reports, the spring bloom metrics (the timing of the start of the bloom, the duration, peak concentration during the bloom period, and "magnitude" or total chl-a produced during the bloom period) relied mainly on the accuracy of the Gaussian fit, which was subject to high variability in chl-a concentration and low data coverage, particularly in the north and early in the year. This resulted in an absence of model fits, or problematic fits that may not have accurately captured the interannual anomalies in each region. To reduce the impact of these bad fits on the scorecards, and retrieve information about bloom timing and intensity, a new set of a metrics were recently proposed: spring bloom peak timing and fall bloom initiation, and "seasonal" averages, where the season boundaries are region-specific and based on the climatology of the spring and fall bloom periods observed over the time series (See Figure A.1, and Blais et al., in prep). While the spring metrics are still derived from a Gaussian fit, we now report on the peak of the curve instead of its initiation, as it does not require a subjective threshold (i.e., percentage of maximum chl-a) and it remains robust to small variation in chl-a early in spring. All fits were visually inspected to ensure that the bloom peak timing was accurately captured by the model, and the input parameters were adjusted if necessary.

The fall bloom period is less predictable than the spring bloom as its signal is not as large as in the spring, and satellite data are more sparse due to cloud cover. Rather than a Gaussian model, a threshold method was used to determine the start of the bloom as the day of year when chl-a concentration surpasses 105% of the annual median and remains above this threshold for 14 consecutive days (Layton et al. 2022). In this case we used the LOESS-smoothed data spanning between day of year 151 and 365 with the initiation occurring between day of year 151 to 270. The timing of the fall bloom initiation was reported rather than the peak, as the peak may occur late in the year when data coverage is poor. Annual times series at daily resolution and the corresponding spring Gaussian and fall threshold fits are available at github.com/BIO-RSG/PhytoFit/blob/master/verified_fits.

The mean chl-a for each region-specific "season" was calculated as an average of the daily chl-a concentrations within that season, weighted by daily percent coverage. Note that in this calculation, daily chl-a concentrations correspond to the averages calculated using absolute (i.e. not log-transformed) values within the polygons, after filtering outlying pixels. Data coverage is very sparse or non-existent in the Labrador Sea from November to January (see Figure A.1). Days with valid data that have low coverage (<20%), a common occurrence early or late in the year, might not be representative of the overall conditions. Sea ice also impacts the quality of the data and may introduce artifacts close to the ice edge (Bélanger et al. 2007). Although weighting points by percent coverage lessens the impact of low data coverage, extra caution must be used when interpreting results in late fall or winter due to these issues.

2.3.6 Access to data products

Data products presented in the figures of this document are available on request to the corresponding author. The satellite ocean colour data can be found in Phytofit (https://cioosatlantic.ca/phytofit), and the bloom metrics (i.e. bloom timing and weighted "seasonal" averages, see Figure 9) are available in the PhytoFit github repository (https://github.com/

BIO-RSG/PhytoFit/tree/master/verified_fits/modisaqua). All the chemical data are available at Ocean Carbon Data System (OCADS).

3 Results and Discussion

3.1 Transient tracers CFC-12 and $\mathrm{SF_6}$

During the second half of the twentieth century, the atmospheric burden of CFCs increased steadily, due mainly to their widespread use as refrigerants and aerosol propellants. The invasive atmospheric flux of these mostly inert gases provided an excellent record of ocean circulation, and profiles of dissolved CFC-12 concentration have been measured annually along the AR7W line since 1991 (Figure 4). As a consequence of restrictions on the manufacturing and use of ozone-depleting substances introduced in 1989, the atmospheric mixing ratio of CFC-12 has been in decline since 2003 and its capacity at tracking recent ventilation episodes has become limited. Unfortunately, the instrument malfunctioned in 2022 and 2023, resulting in a lack of CFC-12 data for those years (Figure 4). Measurements of an alternative transient tracer, $\mathrm{SF_6}$, were introduced in 2011. There has been a rapid, near-linear increase in atmospheric $\mathrm{SF_6}$ since 2011 (+0.08 $\mathrm{fmol\ kg^{-1}\ y^{-1}}$) and it is reflected in the dissolved concentration profiles of the NV-LSW (Figure 4). Data from 2023 requires additional quality control and is not yet available.

3.2 Total inorganic carbon and pH

The Labrador Sea hosts a strong "solubility pump": atmospheric anthropogenic $\mathrm{CO_2}$ is sequestrated to the deep ocean by chemical and physical processes. The depth of the NV-LSW varies from year to year, ranging from 500 m to over 2000 m. TIC concentration increased by 0.84 $\mathrm{\mu mol\ kg^{-1}\ y^{-1}}$ from 1996 to 2023 (Figure 3). As a result, the pH decreased by 0.09 pH units during the same period (Figure 3) representing a decline rate of 0.003 $\mathrm{y^{-1}}$. Trends between 1996 and 2023 were highly significant with a correlation coefficient, r^2, explaining respectively 97% and 80% of the variance in TIC and pH, respectively. Notably, the increasing trend in TIC concentration from 2019 to the 2022 peak was lower overall at 0.51 $\mathrm{\mu mol\ kg^{-1}\ y^{-1}}$ (not shown). Arctic outflow and the local uptake of anthropogenic $\mathrm{CO_2}$ in the deep-convection region of the Labrador Sea are major controlling mechanisms for the state of ocean acidification in the Northwest Atlantic. The observed progress of acidification affects not only the local region but also downstream areas. The Arctic water inflows to the highly productive regions in the Northwest Atlantic, which have important commercial fisheries and make these regions more susceptible to future ocean acidification than other regions (Azetsu-Scott et al. 2010).

3.3 Temperature in the top 100 m

Because the timing of the cruise affects the average temperature for a given region and year, removal of 1998, 1999, 2002, 2003, and 2020 (due to later-than-usual sampling dates, Figure 2) from the reference period (1999-2020) lowered it by about 0.2 ℃ with little effect on the anomaly

patterns (not shown here). AR7W-W exhibited a lower temperature in the top 100 m (mean of 0.8 °C) than AR7W-C (mean of 3.8 °C) and AR7W-E (mean of 2.2 °C) due to the inflow of Arctic water (Figure 5). The warmest years occurred in 2000 (AR7W-W, +1.71 standard deviations from the mean, unitless), 2019 (AR7W-C, +1.54), and 2008 (AR7W-E, +2.08) (Figure 5). The coolest years occurred in 2007 (AR7W-W, -1.36), 2018 (AR7W-C, -1.48), and 2011 (AR7W-E, -1.36).

AR7W-W and AR7W-C showed year-to-year variability between 2019 and 2023 with 2019 being the warmest recorded anomaly in AR7W-C. In 2023, AR7W-W exhibited near-normal temperatures, while AR7W-C showed temperature higher than normal. AR7W-E showed negative anomalies in 2022 and 2023, a trend that started in 2011 (except 2016 and 2019), with less intensity in recent years. Unfortunately, the lack of data in 2020, and a late mission in 2021, did not allow confirmation of these trends.

3.4 Nutrients

All near-surface nutrient concentrations (i.e., 0–100 m, nitrate, phosphate, and silicate) exhibited inter-annual variations between 1997 and 2010, followed by three years (2011 to 2013) of near or below average nutrient levels for all regions, except for silicate (AR7W-W, 2011) and phosphate (AR7W-C, 2013) (Figure 6). From 2014 to 2018, all nutrients levels were above normal except for nitrate and phosphate in 2015 in AR7W-C. While no patterns are observed between nutrients and regions before 2011, all regions and nutrients anomalies were correlated between 2011 and 2019.

Since 2019, surface nitrates show negative trends in all three regions, except in AR7W-E in 2022 (Figure 6). The same year, a record-low in nitrate was measured in AR7W-C. The same trends were observed in phosphate anomalies between 2019 and 2023 with lower than usual concentrations in both AR7W-W and AR7W-C, and a record low phosphate in AR7W-C in 2023. Silicate levels show a different pattern with more variability than nitrate and phosphate levels. AR7W-W showed lower than normal silicate levels since 2019 with a record low in 2022. Silicate levels were close to normal in AR7W-C. In 2019, silicate was lower than normal in AR7W-E and higher than normal in 2022 and 2023.

Deep nutrients (>100 m) showed a different pattern than the surface nutrients in agreement with the hydrodynamics of the Labrador Sea and the surface-layer biological activity (Figure 7). Deep nutrients levels are less impacted by the timing of the mission as they are not consumed by phytoplankton and microbial remineralization at depth replenishes the nutrient pool. Deep nutrients anomalies showed large interannual variability between 1999 and 2018 (Figure 7). Interestingly, most of the record-high levels occurred in the first half of the time series, except for nitrate in AR7W-C (2018), and nitrate and silicate in AR7W-W, which occurred in 2015, a notable year given an unusually large bloom of *Phaeocystis spp.* (Devred et al. 2024). On the other hand, record-low levels of nutrients occurred after 2009. While no clear trend has emerged for the scorecards, since 2019 all deep nutrients have showed below-average levels, except for nitrate in AR7W-C in 2022, which was near normal. However, this trend should be interpreted with caution given that no data from 2020 and 2021 are included. It is noteworthy that these below-average levels of nutrients that started in 2019 coincided with the trend for surface nutrients (Figures 6 and 7).

3.5 In situ chlorophyll-a concentration

In general, the AR7W-E region has high levels of integrated chl-a with a mean of 394 $\mathrm{mg\ m^{-2}}$ from 1999 to 2020 (Figure 8), and is dominated by nanophytoplankton with low concentrations of picophytoplankton. Conversely, AR7W-C is a region with low integrated chl-a (165 $\mathrm{mg\ m^{-2}}$) and a low proportion of nanophytoplankton, with high concentrations of picophytoplankton. AR7W-W exhibits the lowest concentrations of integrated chl-a (122 $\mathrm{mg\ m^{-2}}$) and micro- and nano-phytoplankton dominates the phytoplankton assemblage, with low biomass of picophytoplankton. Upper ocean (< 100 m depth) phytoplankton sampled on the AR7W section in spring and early summer between 1999 and 2022 showed region-specific characteristics (Li and Harrison 2014; Fragoso et al. 2016; Devred et al. 2024).

Integrated chl-a shows a low frequency variability with a given trend (above or below average) that remains for several years at a time. In that respect, the time series for AR7W-W and AR7W-C show two periods of lower-than-normal levels, from about 2001 to 2005 and from 2014 to 2019, while the remaining periods show above-normal values. Record-high levels of integrated chl-a occurred in 2022 in AR7W-W and in 2015 in AR7W-C. Both years corresponded to the very large blooms of *Phaeocystis spp.* (Devred et al. 2024). AR7W-E showed a different pattern than the two other regions, with lower than normal values between 2004 and 2008, followed by a period of large interannual variability (2009 to 2013, 2009 being the record high). Since 2014, integrated chl-a has been lower than average.

Regarding the period of interest in the current report (2019-2023), integrated chl-a showed lower than normal levels in 2019 in all three regions, continuing a trend that started in 2014 (except in AR7W-C in 2015, Figure 8). This trend was also observed in 2022 and 2023 in AR7W-E, although the integrated chl-a was close to normal in 2023. AR7W-W and AR7W-C showed higher than normal levels in 2022 and 2023, with a record high value in 2022 in AR7W-C.

Integrated chl-a levels do not necessarily agree with nutrients concentrations, which can be somewhat explained by the timing of the missions (Figure 2). For instance, in 2013, the mission sampled the transect at the peak of the bloom (as indicated by satellite ocean colour), resulting in high integrated chl-a and low nutrients, likely depleted by phytoplankton consumption. Conversely, in 2014, the mission sampled the AR7W before or at the start of the spring bloom, when chl-a concentration was low and nutrients levels high. Similarly, both 2022 and 2023 missions in AR7W-W and in AR7W-C occurred at the peak of the spring bloom (Figure 2), corresponding to high integrated chl-a values and low nutrients values.

3.6 Satellite-derived chlorophyll-a and bloom indices

Satellite-derived chl-a allows observation of the Labrador Sea all year long, but is limited by sea ice and cloud cover. The main advantage of the satellite is that information on phytoplankton biomass can be reported when sea-going missions have been cancelled. Here we report on the timing of the spring and fall blooms, and the annual and seasonal mean chl-a in the three regions of interest.

The timing of the spring bloom peak is highly variable and depends on several factors, including the thermal stratification, the amount of nutrients, the light available for photosynthesis, and the

grazing pressure. The spring bloom generally occurs first in AR7W-E (day of year (doy) 135 on average), then in AR7W-W (doy 153 on average) and shortly after in AR7W-C (doy 160 on average) (Figure 9). There are no long term trends observed in the timing of the spring bloom but rather a strong interannual variability. Following the record-late spring bloom in 2018 in AR7W-W, both 2019 and 2020 also showed a late bloom, while 2021, 2022 and 2023 showed an earlier than normal bloom peak timing. In AR7W-C, the bloom was late from 2019 to 2021, the later year exhibiting the record-late bloom, which was followed by a record-early bloom in 2022. In 2023, the spring bloom occurred later than normal. In fact, the 2022 bloom was the only one observed to occur earlier than normal since 2015. Note that in both 2015 and 2022, very large and unusual blooms of *Phaeocystis spp.* were observed (Devred et al. 2024). In AR7W-E, both 2019 and 2021 showed earlier than normal bloom initiation, while it was later than normal for the other years. The spring bloom in 2023 was the record-late timing in AR7W-E.

A secondary bloom occurs in the fall, less intense than the spring one, triggered by the replenishment in nutrients of the surface-lit layer by storm-induced vertical mixing when light is still sufficient to stimulate phytoplankton productivity. Similar to the spring bloom peak timing, the fall bloom initiation is very variable over the time series and for each region. Overall, the fall bloom timing has been earlier than normal since 2012, except for a few late years in each regions. In AR7W-W, the bloom was earlier than normal in 2019, 2020, and 2023, with a record early initiation in 2023. The bloom timing was near normal in 2021 and later than normal in 2022. In AR7W-C, the fall bloom occurred earlier than usual from 2019 to 2023, however no fall bloom was observed in 2021. In AR7W-E, the fall bloom timing showed a similar pattern to AR7W-W, with an extremely late fall bloom in 2022 (anomaly of +1.41), however the timing was near normal in 2023.

Annual and spring chl-a average anomalies show correlations in all three regions, suggesting that the spring bloom drives the annual production. The mean annual and seasonal chl-a show high interannual variability. Examining the anomalies in recent years (2019 to 2023), AR7W-W exhibited a record high annual chl-a average (+1.99) despite lower than average levels of nitrate and silicate, suggesting that the ecosystem is not nutrient-limited. The mean annual chl-a was above average in all three regions in 2023. AR7W-C showed above normal chl-a in 2022, in particular in spring, due to an anomalously large bloom of *Phaeocystis spp.* AR7W-E showed a record low anomaly in 2020 when mean chl-a was below normal in all seasons except in summer with a relatively high anomaly. In winter, 2022 showed a record-high mean chl-a in AR7W-E. An exceptionally large early bloom occurred in 2018 in AR7W-W and AR7W-C (+3.92 and +3.97, respectively) impacting the entire reference period and reducing the anomalies for all the other years.

3.7 Mesozooplankton

C. finmarchicus copepods dominate the mesozooplankton biomass in AR7W-C, while they and their congeners *C. glacialis* and *C. hyperboreus* contribute about one third each of total biomass on the shelves (AR7W-W and AR7W-E) (Head et al. 2003). *C. finmarchicus* total abundance is greatly influenced by the abundance of young stage copepodites, which develop from eggs laid that have overwintered as pre-adults in the deep central basin and re-ascended in spring. The phytoplankton spring bloom provides the fuel required for egg-laying and the development of

subsequent population, so that regional differences in spring bloom dynamics lead to differences in the timing of the development of *C. finmarchicus* populations. Since spring blooms are generally earlier and more intense in AR7W-E than elsewhere, *C. finmarchicus* abundance is generally higher in AR7W-E than in other regions of the Labrador Sea at the time of sampling (Figure 10).

In AR7W-W, 2011 had an exceptionally high abundance of *C. finmarchicus*, which remains unexplained (Figure 10). For the rest of the time series, abundances have been variable, with two higher-than-average values in 2001 and 2019 and a sustained period of relatively-low abundance occurring between 2004 and 2008. The high abundance in 2019 was mostly due to the large number of younger stages, which is reflected in the higher-than-average %PDI typical of a post-phytoplankton bloom sampling. In AR7W-C, development of the spring bloom and the relatively late development of *C. finmarchicus* result in higher abundance of *C. finmarchicus* in summer than in spring (Figure 10). Young stages were seldom very abundant, perhaps due to high mortality (Head et al. 2015) except for the summer of 1995, with an exceptionally higher total abundance year. There was no trend in spring total abundance for *C. finmarchicus* between 1997 and 2023. The high abundance in 2022 reflects the extension of the large *Phaeocystis* bloom favoring the growth of young copepodite stages as showed by a higher PDI anomaly. In AR7W-E, there was one exceptionally high *C. finmarchicus* abundance value in May 2006, the cause of which is unclear.

High climatological abundance of *C. glacialis* and *C. hyperboreus* in AR7W-W ($2x10^3$ and $4x10^3$, respectively) and AR7W-E ($1x10^3$ and $3x10^3$) compared to AR7W-C ($3x10^2$ and $1x10^3$) may result from the transport of individuals in the inflows, since neither species have a local source of overwintering population. The abundance of both species has generally shown considerable year-to-year variability, but with sustained periods of low abundance for *C. glacialis* on both shelves since 2014 with the exception of 2019 where abundance were higher or around the average in all regions. Sustained periods of high abundance for *C. hyperboreus* occurred in AR7W-E between 2009 and 2012 while low abundance occurred in AR7W-W between 2012 and 2018 (Figure 10).

Pseudocalanidae spp. have been generally more abundant than average in AR7W-C since 2008, whereas a general decreasing trend was observed in AR7W-W and AR7W-E between 2014 and 2018 (Figure 10). Since 2019 abundance in all 3 regions are either close to or higher than the average with the exception of AR7W-E in 2022 which remained below but close to normal conditions. The extension of a large bloom of the phytoplankton species *Phaeocystis* (Devred et al. 2024) was generally limited to AR7W-E and the middle of AR7W-C at that time of year, and may explain the large abundance of *Pseudocalanidae*. In contrast, *Oithonidae* remained persistently less abundant than average in AR7W-C since 2013, while the decrease in abundance on both shelves became more prevalent around 2014 (AR7W-W) and 2015 (AR7W-E) (Figure 10). In AR7W-W the *Oithona* abundance was significantly higher than average in 2022 and 2023 and close to the average in AR7W-E.

Up to 2013, *Euphausiid* showed large interannual variability in the three regions of interest (Figure 10). Between 2014 and 2019, *Euphausiid* abundance was consistently lower than average in all regions, except in AR7W-W in 2019 which was slightly higher than average. Abundance has been low to normal since 2022 in AR7W-E, high in AR7W-W with the second highest abundance on record in 2022, and high in 2022 and low in 2023 in AR7W-C. Amphipods,

mostly represented here by *Parathemisto libellula*, showed lower-than-average abundances throughout the LS since 2016, following a decade-long period of higher interannual variability. In 2023, Amphipoda abundances reached record lows in AR7W-E and AR7W-C and the third lowest abundance on record in AR7W-W.

4 Summary

The Atlantic Zone Off-Shelf Monitoring Program (AZOMP) provides observations on ocean climate and plankton variability within the Labrador Sea and adjacent shelves affecting ecosystems of Atlantic Canada and climate from a regional to global scale. In the Labrador Sea, surface heat losses in winter result in the formation of dense waters, which spread across the ocean, ventilating the deep layers, thus contributing to the global ocean-overturning circulation.

CFC-12 concentration experienced a decline from 2019-2020, but the lack of sampling in 2021 and instrument malfunction from 2022 to 2023 could not confirm the continuing downward trend. SF_6 concentration continued increasing linearly at a rate of 0.08 $\mathrm{fmol\ kg^{-1}\ y^{-1}}$, but the 2023 data requires additional quality control before reporting. TIC concentrations from the NV-LSW in the central Labrador Sea have continued to increase as in previous years, though at a slower rate (0.84 $\mu\mathrm{mol\ kg^{-1}\ y^{-1}}$ from 1996 to 2023, but only 0.51 $\mu\mathrm{mol\ kg^{-1}\ y^{-1}}$ from 2019 to the 2022 peak). The increase resulted in pH levels continuing their declining trend (0.003 pH units per year). Average surface layer temperature in the AR7W-C has fluctuated between anomalously low (2022) and high (2019, 2023) values, whereas the shelves (AR7W-W and AR7W-E) have been near-normal except for the cold period in 2022.

Strong inter-annual variability was observed in surface nutrient concentrations, which are consistent among regions. From 2014 to 2018, there were positive anomalies in all regions, with the exception of nitrate and phosphate in AR7W-C in 2015. Negative anomalies have been observed since 2019 in AR7W-W and AR7W-C for all nutrients except for silicate in AR7W-C in 2022, which was normal. In contrast in AR7W-E, silicate concentrations rebounded in 2022-2023, and nitrate and phosphate anomalies were positive in 2022 and negative again in 2023. Deep nutrient concentrations also experienced high interannual variability, but have been negative across all regions since 2019. Chl-a concentrations have followed an inverse pattern to surface nutrients, with lower than normal concentrations for all three regions since 2014, except for the anomalously high concentration in 2015 in AR7W-C, and high concentrations in AR7W-W and AR7W-C in 2022-2023. The high chl-a anomalies and below-normal nitrate and phosphate anomalies in AR7W-C in 2015 and 2022 were associated with an intense phytoplankton bloom consisting mainly of *Phaeocystis spp.* which was identified from shipboard observations. Recurrent earlier sampling dates from year to year may partly explain the observed negative anomalies in chl-a concentrations, since sampling may have occurred before the start of the seasonal spring bloom. Ocean color metrics (spring peak timing, fall bloom initiation, and annual and seasonal averages) showed no obvious trends over time or correlations between regions, though correlations between spring and annual averages suggest the spring bloom is the biggest contributor to overall annual biomass production. Satellite observations are impacted by cloud and ice cover as well as low sun angle at such high latitudes, resulting in data gaps that might miss the peak of the bloom in a given year and region and bias the metrics.

With the exception of *Pseudocalanus spp.* and Amphipoda, which exhibited high and low abundance anomalies respectively, other taxa do not show clear trends during the 2019-2023 period. In AR7W-W and AR7W-C, the higher than average %PDI in *C. finmarchicus* may have been linked in part to their seasonal life-cycle where the populations were consistently more advanced in development than the average. The AR7W-E region, generally sampled later in the bloom season, showed a population growth rate which was slower or close to the average.

The chemistry and biology of the Labrador Sea show strong regional and interannual variation. The time period of 2019 to 2023 was marked by a steady increase in TIC, decrease in pH, and an increase in SF_6. Furthermore, there was a shift in nutrients and chl-a, with a decline in nutrient concentrations both in surface waters and at depth, and an increase in surface chl-a that could be partially explained by the timing of the mission relative to the bloom. Satellite ocean colour revealed spring and fall bloom timing that was highly variable, with implications for zooplankton abundance. As our ocean continues to experience shifts in average conditions, long-running and consistent time series are critical to understand the wide-ranging impacts on ocean ecosystems.

5 Acknowledgements

The authors thank the sea-going staff of the Bedford Institute of Oceanography and the officers and crew of the Canadian Coast Guard ships Amundsen and Captain Jacques Cartier as well as the UNOLS research vessel Atlantis. Jay Barthelotte, Robert Benjamin, Jay Bugden, Diana Cardoso, Carla Caverhill, Terry Cormier, Melissa Falkner, Jennifer Field, Yuri Geshelin, Chris Gordon, Pascal Guillot, Adam Hartling, Dave Hebert, Flo Hum, Jeff Jackson, Matt Lawson, Chantelle Layton, Dave Levy, Richard Nelson, Kevin MacIsaac, Kevin Pauley, Tim Perry, Cathy Porter, Steve Punshon, Maddison Proudfoot, Peter Thamer, Christiane Theriault, Mike Vining, and Kristen Wilson contributed to sample collection, sample analysis, data analysis, data management, and data sharing.

6 References

Astthorsson, O.S., and Gislason, A. 2003. Seasonal variations in abundance, development and vertical distribution of Calanus finmarchicus, C. hyperboreus and C. glacialis in the East Icelandic Current. Journal of Plankton Research 25(7): 843–854.

Azetsu-Scott, K., Clarke, A., Falkner, K., Hamilton, J., Jones, E. P., Lee, C., Petrie, B., Prinsenberg, S., Starr, M., and Yeats, P. 2010. Calcium carbonate saturation states in the waters of the Canadian Arctic Archipelago and the Labrador Sea. Journal of Geophysical Research 115(C11021).

Azetsu-Scott, K., Jones, E. P., Yashayaev, I., and Gershey, R.M. 2003. Time series study of CFC concentrations in the Labrador Sea during deep and shallow convection regimes (1991–2000). Journal of Geophysical Research: Oceans 108(C11).

Becker, S., Aoyama, M., Woodward, E. M. S., Bakker, K., Coverly, S., Mahaffey, C., and Tanhua, T. 2020. GO-SHIP repeat hydrography nutrient manual: The precise and accurate determination of dissolved inorganic nutrients in seawater, using continuous flow analysis methods. Frontiers in Marine Science 7: 581790.

Bélanger, S., Ehn, J.K., and Babin, M. 2007. Impact of sea ice on the retrieval of water-leaving reflectance, chlorophyll a concentration and inherent optical properties from satellite ocean color data. Remote Sensing Env. 111(1): 51–68.

Caldeira, K., and Wickett, M.E. 2003. Anthropogenic carbon and ocean pH. Nature 425: 365.

Clay, S., Layton, C., and Devred, E. 2021. PhytoFit: First release (v1.0.0).

Clay, S., Peña, A., DeTracey, B., and Devred, E. 2019. Evaluation of satellite-based algorithms to retrieve Chlorophyll-a concentration in the Canadian Atlantic and Pacific oceans. Remote Sens. 11(22).

Devred, E., Wilson, K. L., Perry, T., Hardy, M., Brosnahan, M., and Ringuette, M. 2024. Identification and validation of phytoplankton taxonomic assemblages derived from pigment signatures using samples collected in the Labrador Sea from 2014 to 2022. Can. Tech. Rep. Fish. Aquat. Sci. 3596: viii + 55 p.

Dickson, A. G., Sabine, C. L., and Christian, J.R.(Eds.). 2007. Guide to best practices for ocean CO2 measurements. PICES Special Publication 3.

Elzhov, T.V., Mullen, K.M., Spiess, A.-N., and Bolker, B. 2023. Minpack.lm: R interface to the levenberg-marquardt nonlinear least-squares algorithm found in MINPACK, plus support for bounds.

Feely, R. A., Sabine, C. L., Lee, K., Berelson, W., Kleypas, J., Fabry, V. J., and Millero, F.J. 2004. Impact of anthropogenic CO2 on the CaCO3 system in the oceans. Science 305(5682): 362–366.

Fragoso, G. M., Poulton, A. J., Yashayaev, I. M., Head, E.J.H., Stinchcombe, M. C., and Purdie, D.A. 2016. Biogeographical patterns and environmental controls of phytoplankton communities from contrasting hydrographical zones of the Labrador Sea. Progress in Oceanography 141: 212–226.

Haine, T. W. N., and Hall, T.M. 2002. A generalized transport theory: Water-mass composition and age. Journal of Physical Oceanography 32(6): 1932–1946.

Hall, T. M., Haine, T. W. N., and Waugh, D.W. 2002. Inferring the concentration of anthropogenic carbon in the ocean from tracers. Global Biogeochemical Cycles 16(4): 1131.

Harrison, W. G., and Li, W.K.W. 2008. Phytoplankton growth and regulation in the Labrador Sea: Light and nutrient limitation. Journal of Northwest Atlantic Fishery Science 39: 71–82.

Head, E. J. H., Azetsu-Scott, K., Harrison, G., Hendry, R., Li, W., Yashayaev, I., and Yeats,

P. 2008. Changes in environmental conditions and the population dynamics of Calanus finmarchicus in the Labrador Sea (1990-2006).
Head, E. J. H., Gentleman, W. C., and Ringuette, M. 2015. Variability of mortality rates for Calanus finmarchicus early life stages in the Labrador Sea and the significance of egg viability. Journal of Plankton Research 37(6): 1149–1165.
Head, E. J. H., Harris, L. R., and Yashayaev, I. 2003. Distributions of Calanus spp. And other mesozooplankton in the Labrador Sea in relation to hydrography in spring and summer (1995–2000). Progress In Oceanography 59(1): 1–30.
Holm-Hansen, O., Lorenzen, C. J., Holmes, R. W., and Strickland, J.D.H. 1965. Fluorometric determination of chlorophyll. ICES Journal of Marine Science 30(1): 3–15.
Hood, E. M., Sabine, C. L., and Sloyan, B.M.(Eds.). 2010. The GO-SHIP repeat hydrography manual: A collection of expert reports and guidelines, version 1. (IOCCP Report 14), (ICPO Publication Series 134).
Johnson, K. M., Sieburth, J.McN., Williams, P. J.leB., and Brändström, L. 1987. Coulometric total carbon dioxide analysis for marine studies: Automation and calibration. Marine Chemistry 21(2): 117–133.
Jones, P. D., and Hulme, M. 1996. Calculating regional climatic time series for temperature and precipitation: Methods and illustrations. International Journal of Climatology 16(4): 361–377.
Kérouel, R., and Aminot, A. 1997. Fluorometric determination of ammonia in sea and estuarine waters by direct segmented flow analysis. Marine Chemistry 57(3): 265–275.
Layton, C., Devred, E., and Detracey, B. 2022. A comparison of phytoplankton spring bloom fitting methods using MODIS satellite-derived chlorophyll-a concentration for the Maritimes region. Can. Tech. Rep. Hydrogr. Ocean Sci. 340: vii + 22p.
Li, W. K. W., and Harrison, W.G. 2014. The state of phytoplankton and bacterioplankton in the Labrador Sea: Atlantic Zone Off-Shelf Monitoring Program 1994–2013. Can. Tech. Rep. Hydrogr. Ocean. Sci. 302: xviii + 181p.
Lozier, M. S., Li, F., Bacon, S., Bahr, F., Bower, A., Cunningham, S., De Jong, M. F., Steur, de, L., Deyoung, B., Fischer, J., Gary, S., Greenan, B., Holliday, N., Houk, A., Houpert, L., Inall, M., Johns, W., Johnson, H., Johnson, C., and Zhao, J. 2019. A sea change in our view of overturning in the subpolar North Atlantic. Science 363(6426): 516–521.
Lueker, T. J., Dickson, A. G., and Keeling, C.D. 2000. Ocean pCO2 calculated from dissolved inorganic carbon, alkalinity, and equations for K1 and K2: Validation based on laboratory measurements of CO2 in gas and seawater at equilibrium. Marine Chemistry 70(1): 105–119.
Mitchell, M. R., Harrison, G., Pauley, K., Gagné, A., Maillet, G., and Strain, P. 2002. Atlantic Zonal Monitoring Program sampling protocol. *In* Can. Tech. Rep. Hydrogr. Ocean. Sci. 223: iv + 23p.
O'Reilly, J. E., Maritorena, S., Mitchell, B. G., Siegel, D. A., Carder, K. L., Garver, S. A., Kahru, M., and McClain, C. 1998. Ocean color chlorophyll algorithm for SeaWiFS. J. Geophys. Res. 103: 937–953.
Platt, T., and Jassby, A.D. 1976. The relationship between photosynthesis and light for natural assemblages of coastal marine phytoplankton. Journal of Phycology 12: 421–430.
Punshon, S., Azetsu-Scott, K., Sherwood, O., and Edinger, E.N. 2019. Bottom water methane sources along the high latitude eastern Canadian continental shelf and their effects on the marine carbonate system. Marine Chemistry 212: 83–95.
Punshon, S., Childs, D., and Azetsu-Scott, K. 2016. A purge-and-trap gas chromatographic method for shipboard determination of the transient tracers sulphur hexafluoride and

dichlorodifluoromethane in seawater and in air. Can. Tech. Rep. Hydrogr. Ocean Sci. 309: vii + 21p.

Raimondi, L., Matthews, J. B. R., Atamanchuk, D., Azetsu-Scott, K., and Wallace, D.W.R. 2019. The internal consistency of the marine carbon dioxide system for high latitude shipboard and in situ monitoring. Marine Chemistry 213: 49–70.

Raimondi, L., Tanhua, T., Azetsu-Scott, K., Yashayaev, I., and Wallace, D.W.R. 2021. A 30-year time series of transient tracer-based estimates of anthropogenic carbon in the central Labrador Sea. Journal of Geophysical Research: Oceans 126(5): e2020JC017092.

Sabine, C. L., Feely, R. A., Gruber, N., Key, R. M., Lee, K., Bullister, J. L., Wanninkhof, R., Wong, C. S., Wallace, D. W. R., Tilbrook, B., Millero, F. J., Peng, T.-H., Kozyr, A., Ono, T., and Rios, A.F. 2004. The oceanic sink for anthropogenic CO2. Science 305(5682): 367–371.

Wang, Z., Brickman, D., Greenan, B. J. W., and Yashayaev, I. 2016. An abrupt shift in the Labrador Current System in relation to winter NAO events. Journal of Geophysical Research: Oceans 121(7): 5338–5349.

Welschmeyer, N.A. 1994. Fluorometric analysis of chlorophyll a in the presence of chlorophyll b and pheopigments. Limnology and Oceanography 39(8): 1985–1992.

Yashayaev, I., and Loder, J.W. 2017. Further intensification of deep convection in the Labrador Sea in 2016. Geophysical Research Letters 44(3): 1429–1438.

Yashayaev, I., Peterson, I., and Wang, Z. 2021. Meteorological, sea ice and physical oceanographic conditions in the Labrador Sea during 2018. DFO Can. Sci. Advis. Sec. Res. Doc. 2021/042. iv + 26 p.

Yebra, L., Harris, R. P., Head, E. J. H., Yashayaev, I., Harris, L. R., and Hirst, A.G. 2009. Mesoscale physical variability affects zooplankton production in the Labrador Sea. Deep Sea Research Part I: Oceanographic Research Papers 56(5): 703–715.

Yentsch, C.S., and Menzel, D.W. 1963. A method for the determination of phytoplankton chlorophyll and phaeophytin by fluorescence. Deep Sea Research 10(3): 221–231.

7 Tables

Table 1. Atlantic Zone Off-Shelf Monitoring Program sampling missions between 2019 and 2023.

			Number of stations		
Year	**Mission**	**Dates**	**Hydro**	**BIO**	**Net**
2019	AMU2019-001	9 – 21 June	55	7	40
2020	AMU2020-001	28 July – 7 August	62	7	36
2021	Mission cancelled	5 – 15 May	0	0	0
2022	AT4805	10 – 20 May	62	7	28
2023	CAR2023-573	26 May – 6 June	35	0	35

8 Figures

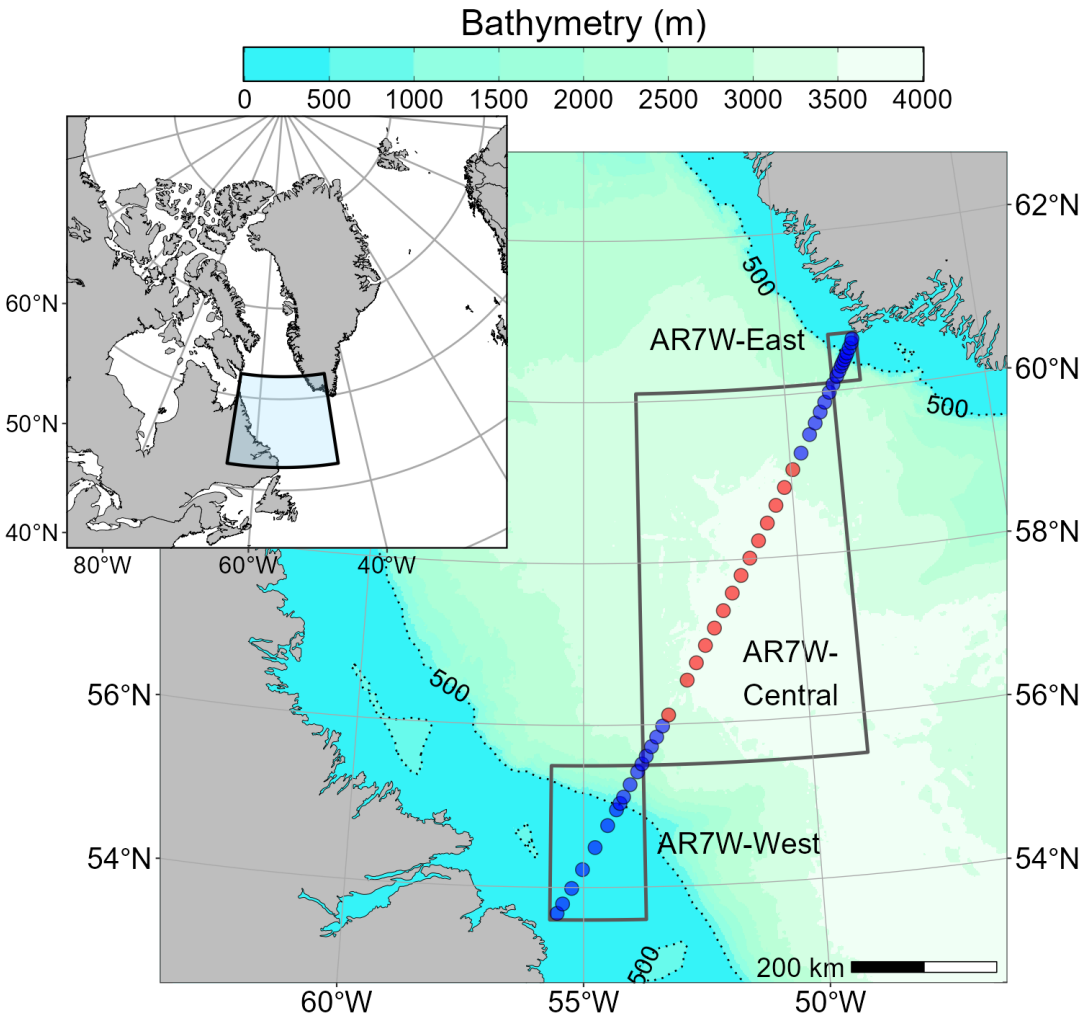

Figure 1. AR7W transect within the Labrador Sea. Blue and red dots represent the location of the core stations. Red stations are used in the calculation of annual averages for TIC, pH, and tracers for the NV-LSW from 150-500 m depth. Boxes correspond to the regions where satellite chl-a concentration is extracted (i.e., AR7W-West, AR7W-Central, and AR7W-East). Dotted black lines correspond to the 500 m isobath.

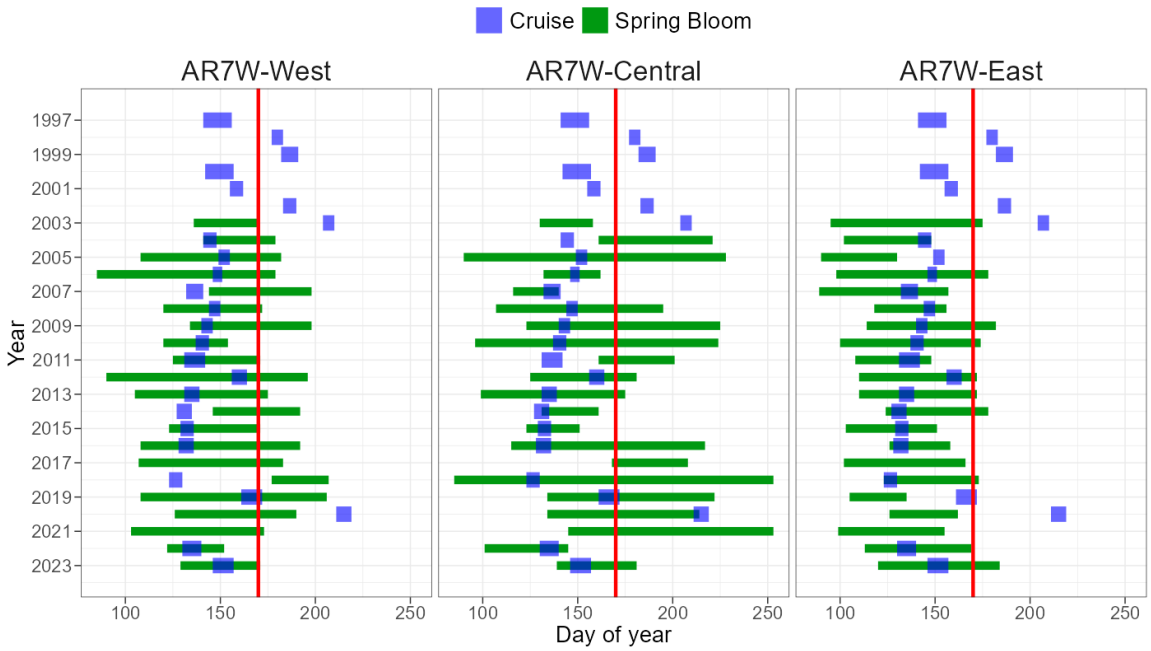

Figure 2. Blue rectangles represent the sampling period (actual occupation of AR7W line) and green rectangles correspond to the duration of the spring bloom within each region as derived from satellite ocean colour for AR7W-West (left), AR7W-Central (middle), and AR7W-East (right). Dates are reported in day of year. Missions in 2019 and 2020 were onboard CCGS Amundsen in late-June and August respectively. The COVID pandemic prevented the execution of the mission in spring 2020. Lack of vessel availability lead to the absence of a mission in 2021. Vertical red line (day of year 170) represents our cutoff date separating early and late missions.

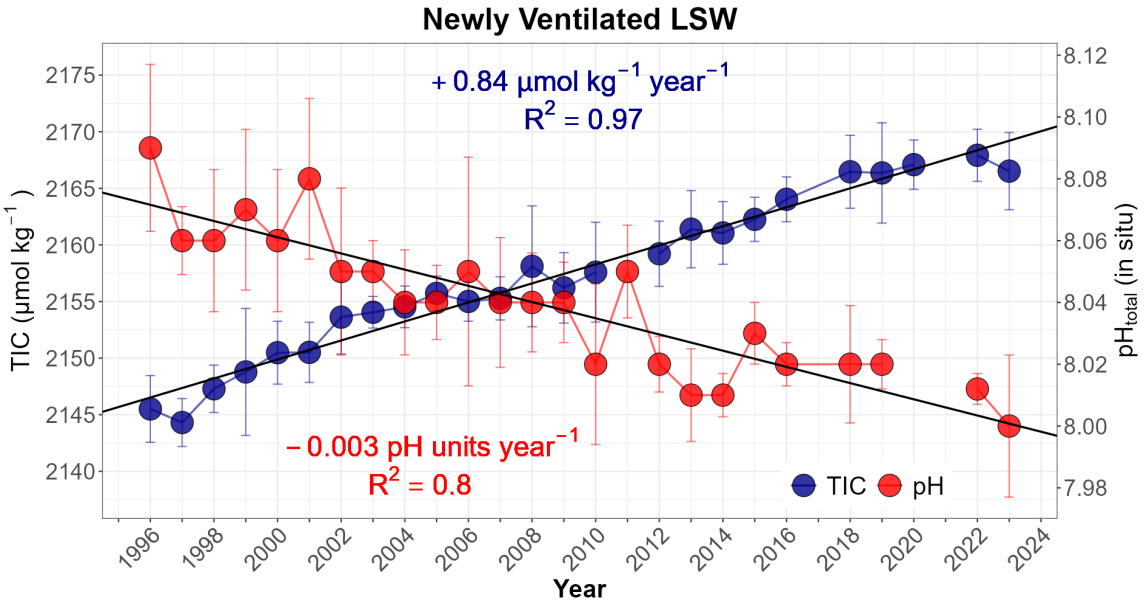

Figure 3. Time series of total inorganic carbon (TIC; blue solid circles) and pH (red solid circles) within the Newly Ventilated Labrador Sea Water (150–500 m depth within 56°N to 59.1°N). Vertical bars indicate one standard deviation and black solid lines correspond to the linear regression of TIC and pH against time for the period 1996-2023.

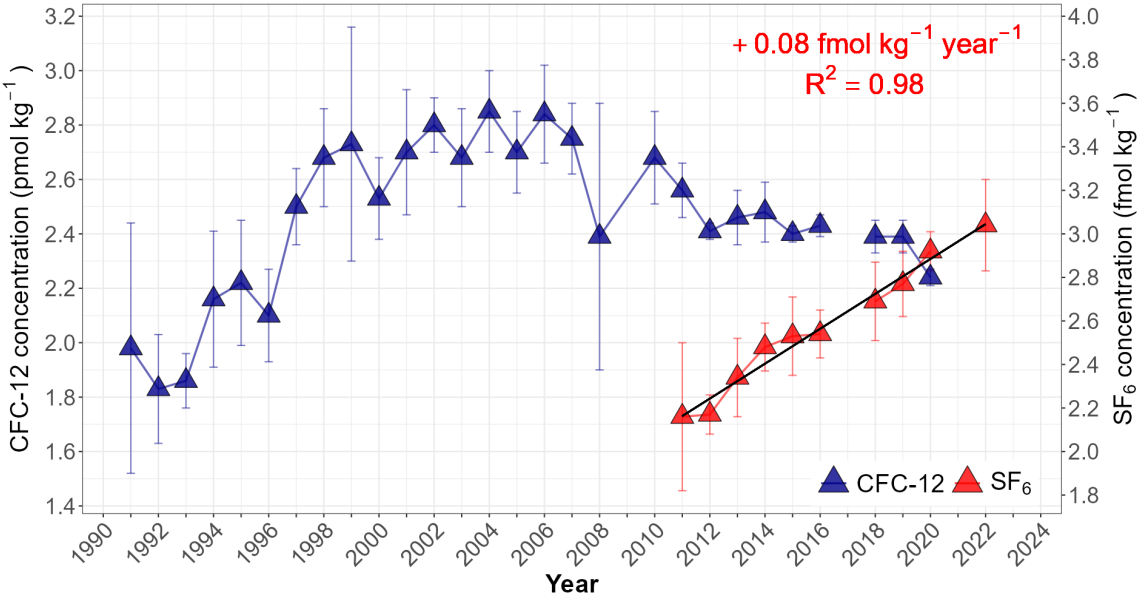

Figure 4. Annual mean concentrations of CFC-12 (blue solid triangles) and $\mathrm{SF_6}$ (red solid triangles) in the Newly Ventilated Labrador Sea Water (150–500 m depth within 56°N to 59.1°N) from 1991 to 2023. Vertical bars indicate one standard deviation and black solid line corresponds to the linear regression of $\mathrm{SF_6}$ against time for the period 2011-2022.

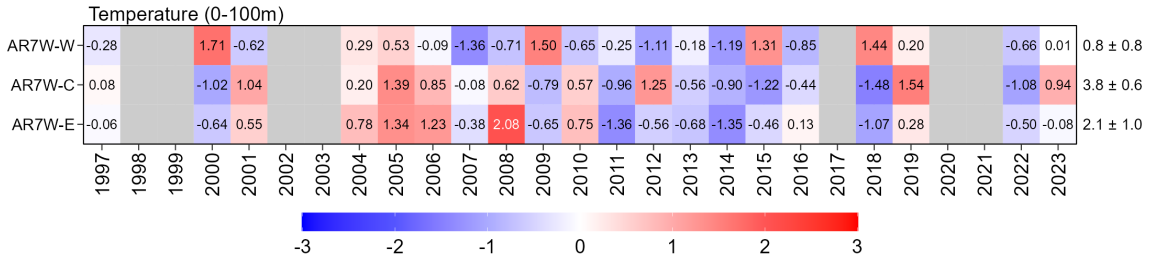

Figure 5. Scorecards for average temperature in the water column (surface to 100 m) measured from the CTD during each bottle firing, from 1997 to 2023 for the AR7W-West (AR7W-W), AR7W-Central (AR7W-C), and AR7W-East (AR7W-E) polygons. Grey boxes indicate no data or late sampling years (not included in the reference period average). Numbers in the scorecard cells represent the annual standardized anomalies. Numbers on the right side indicate the mean values 1999–2020 (i.e., reference, ℃) for a given region as well as the standard deviation (i.e., mean ± standard deviation).

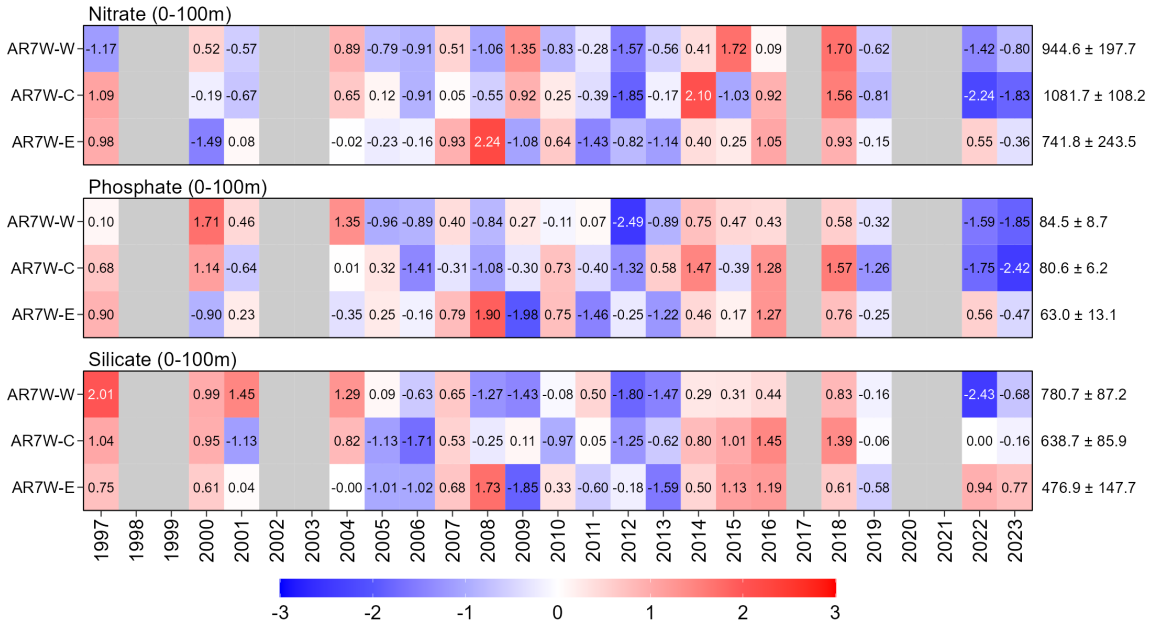

Figure 6. Scorecards for surface nutrients from 1997 to 2023 for the AR7W-West (AR7W-W), AR7W-Central (AR7W-C), and AR7W-East (AR7W-E) polygons. Grey boxes indicate no data or late sampling years (not included in the reference period average). Numbers in the scorecard cells represent the annual standardized anomalies. Numbers on the right side indicate the mean values 1999–2020 (i.e., reference, $\mathrm{mmol\ m^{-2}}$) for a given region as well as the standard deviation (i.e., mean ± standard deviation).

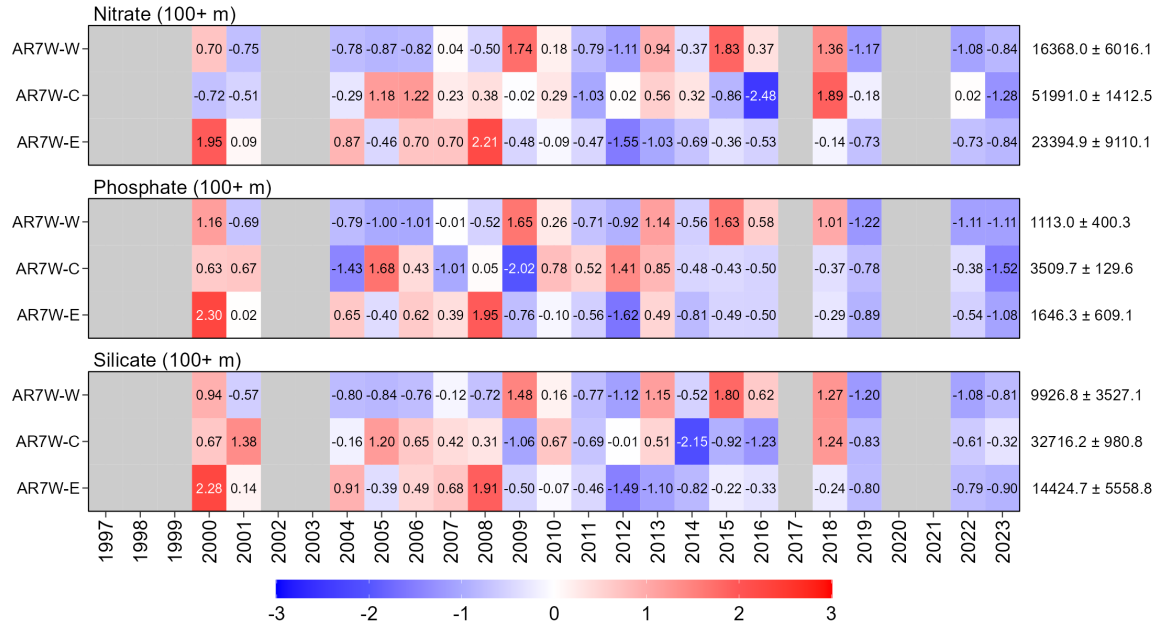

Figure 7. Scorecards for deep nutrients from 1997 to 2023 for the AR7W-West (AR7W-W), AR7W-Central (AR7W-C), and AR7W-East (AR7W-E) polygons. Grey boxes indicate no data or late sampling years (not included in the reference period average). Numbers in the scorecard cells represent the annual standardized anomalies. Numbers on the right side indicate the mean values 1999–2020 (i.e., reference, $\mathrm{mmol\ m^{-2}}$) for a given region as well as the standard deviation (i.e., mean ± standard deviation).

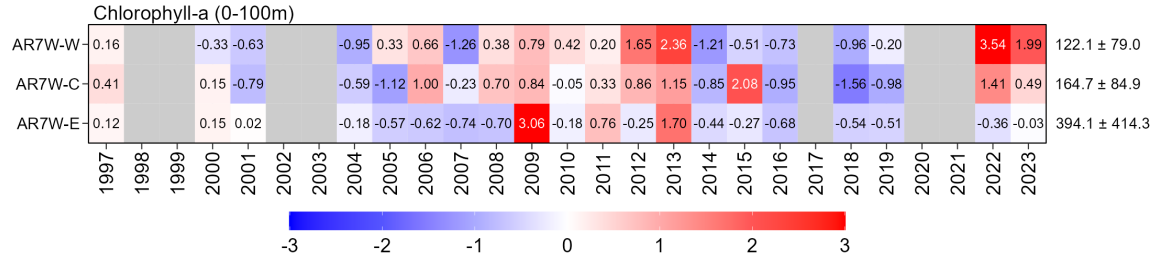

Figure 8. Scorecards for in situ chl-a from 1997 to 2023 for the AR7W-West (AR7W-W), AR7W-Central (AR7W-C), and AR7W-East (AR7W-E) polygons. Grey boxes indicate no data or late sampling years (not included in the reference period average). Numbers within cells represent the annual standardized anomalies. Numbers on the right side indicate the mean values 1999–2020 (i.e., reference, $\mathrm{mg\ m^{-2}}$) for a given region as well as the standard deviation (i.e., mean ± standard deviation).

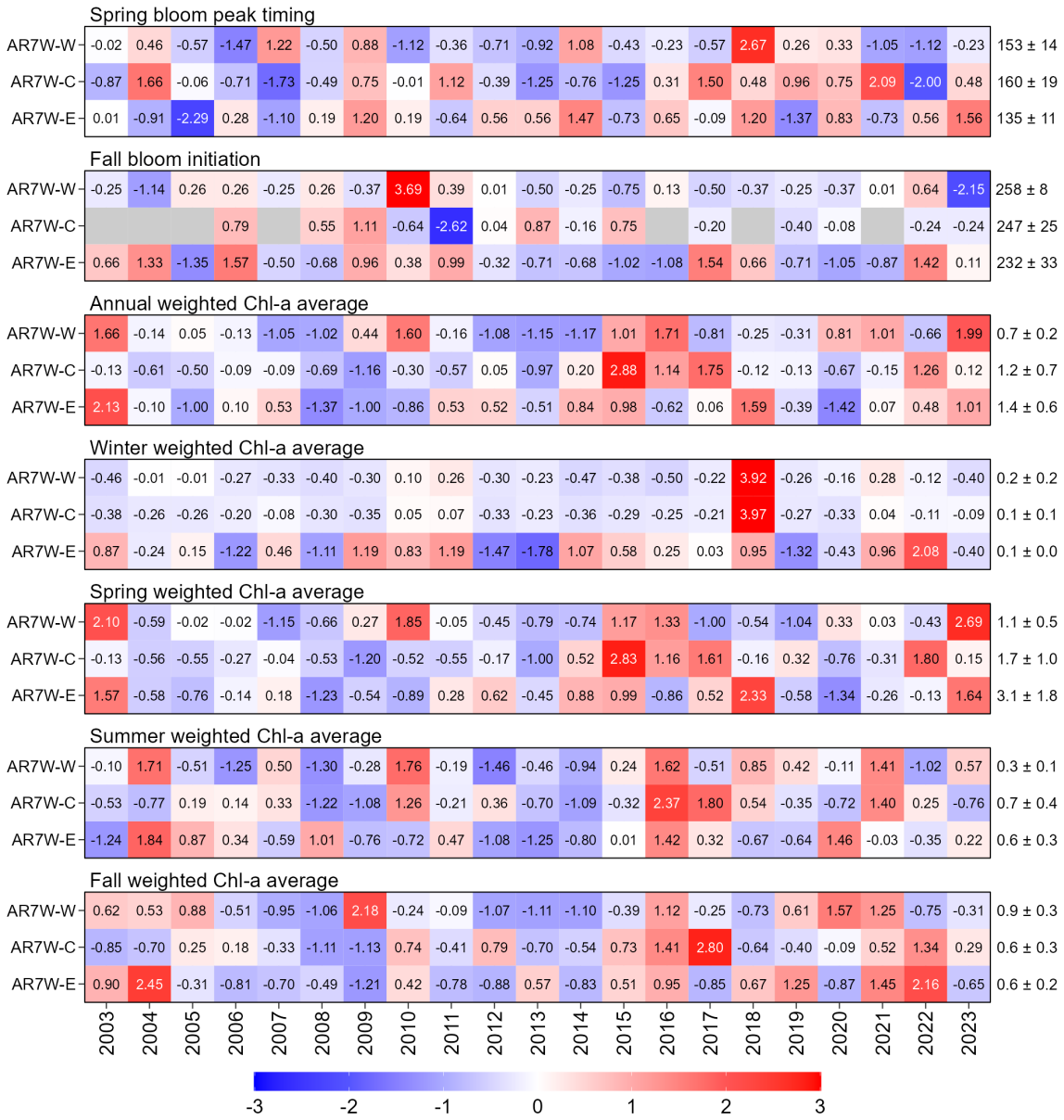

Figure 9. Scorecards for seasonal surface chl-a metrics derived from data retrieved by the MODIS-Aqua satellite sensor (timing is the day of year, and averages are measured in $\mathrm{mg\ m^{-3}}$) from 2003 to 2023 for the AR7W-West (AR7W-W), AR7W-Central (AR7W-C), and AR7W-East (AR7W-E) polygons. Grey boxes indicate no data. Numbers within cells represent the annual standardized anomalies. Numbers on the right side indicate the mean values 2003–2020 (i.e., reference) for a given region as well as the standard deviation (i.e., mean ± standard deviation).

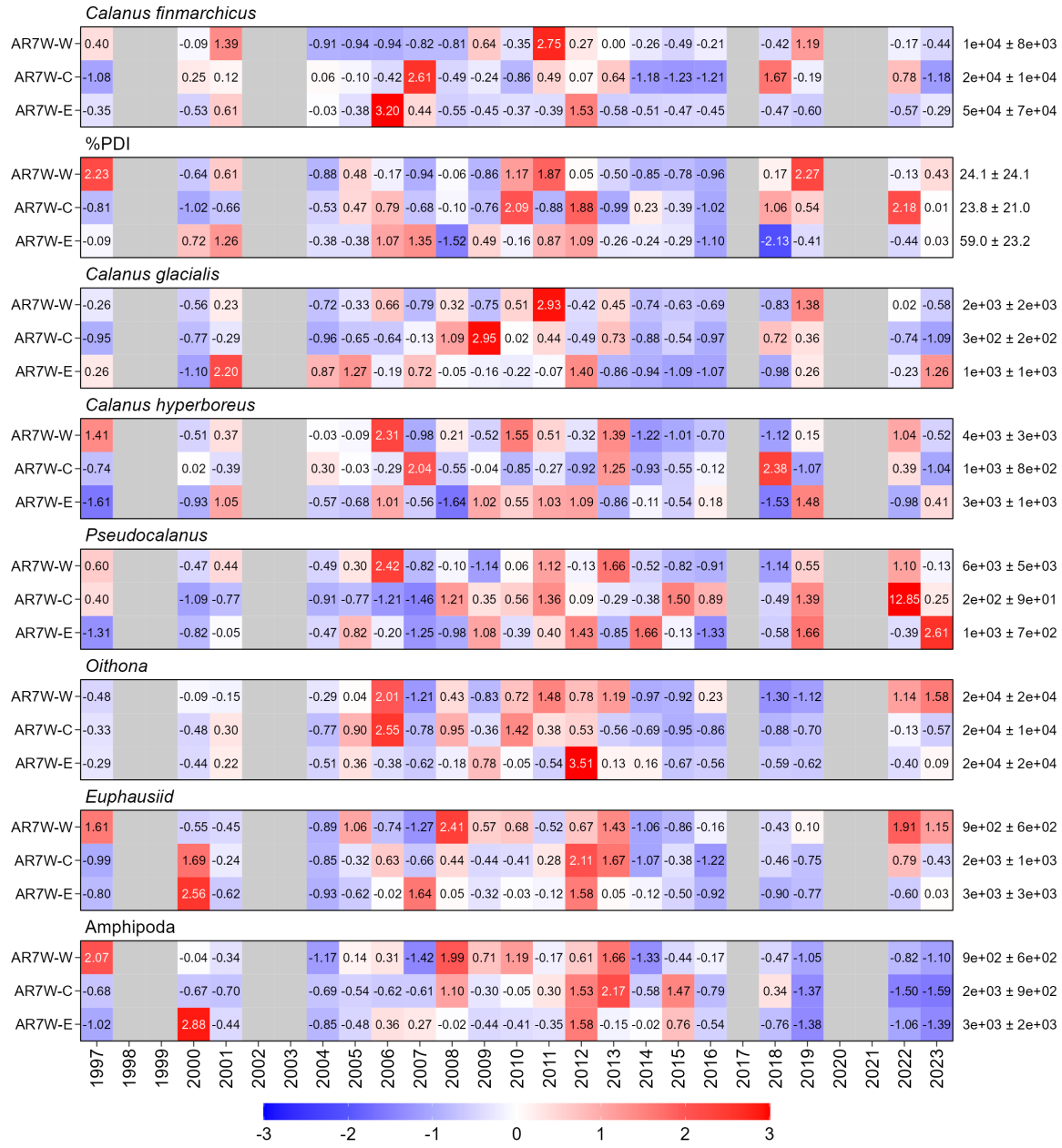

Figure 10. Scorecards for mesozooplankton abundances from 1997 to 2023 for AR7W-West (AR7W-W), AR7W-Central (AR7W-C), and AR7W-East (AR7W-E) expressed as normalized anomalies (dimensionless) based on 1999–2020 reference period. The second panel from the top shows the Population Development Index (%PDI) calculated as the sum abundance of *C. finmarchicus* copepodite CI-CIII * 100 and divided by the sum of all developmental stages. Numbers on the right side indicate the mean values 1999–2020 (i.e., reference period) for a given region as well as the standard deviation (i.e., mean ± standard deviation). Grey cells indicate anomalies were omitted due to late sampling or that no sampling occurred that year due to lack of vessel (2017, 2021).

APPENDIX A Ocean Color Polygon Seasons

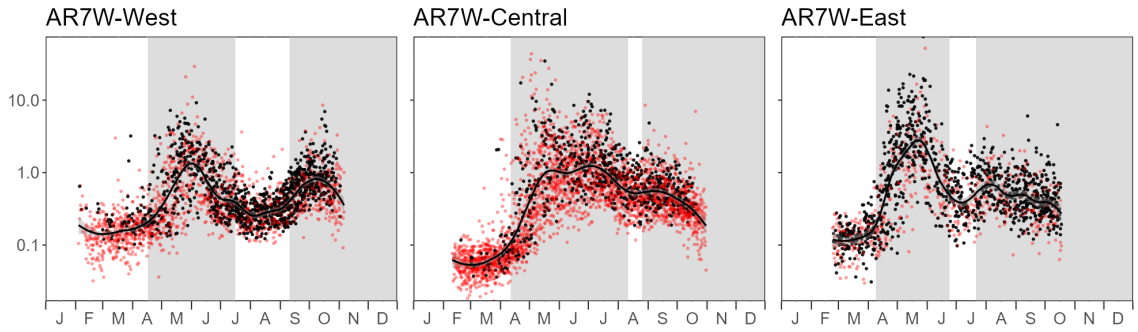

Figure A.1. Time series of daily average concentrations within each Labrador Sea polygon over the climatological period (2003-2020). Grey shaded areas indicate the spring and fall bloom periods (i.e., region-specific “seasons”). White areas indicate the winter and summer “seasons”. Red circles corresponds to daily data coverage of less than 20% of a polygon. Days of the year marking the transition from winter to spring, spring to summer, and summer to fall are 107, 197, and 254 (AR7W-West), 102, 223, and 238 (AR7W-Central), and 99, 175, and 203 (AR7W-East).